

Plots of the cumulative differences between observed and expected values of ordered Bernoulli variates

Mark Tygert

March 26, 2022

Abstract

Many predictions are probabilistic in nature; for example, a prediction could be for precipitation tomorrow, but with only a 30% chance. Given both the predictions and the actual outcomes, “reliability diagrams” (also known as “calibration plots”) help detect and diagnose statistically significant discrepancies between the predictions and the outcomes. The canonical reliability diagrams are based on histogramming the observed and expected values of the predictions; several variants of the standard reliability diagrams propose to replace the hard histogram binning with soft kernel density estimation using smooth convolutional kernels of widths similar to the widths of the bins. In all cases, an important question naturally arises: which widths are best (or are multiple plots with different widths better)? Rather than answering this question, plots of the cumulative differences between the observed and expected values largely avoid the question, by displaying miscalibration directly as the slopes of secant lines for the graphs. Slope is easy to perceive with quantitative precision even when the constant offsets of the secant lines are irrelevant. There is no need to bin or perform kernel density estimation with a somewhat arbitrary kernel.

Keywords: calibration, plot, reliability, diagram, forecast, prediction

1 Introduction

Given 100 independent observations of outcomes (“success” or “failure”) of Bernoulli trials that are forecast to have an 80% chance of success, the forecasts are perfectly *calibrated* when 80 of the observations report success. More generally, given some number, say n , of independent observations of outcomes of Bernoulli trials that are forecast to have a probability p of success, the predictions are perfectly calibrated when np of the observations report success. Needless to say, the actual number of observations of success is likely to vary around np randomly, so in practice we test not whether np is exactly equal to the actual number of observations, but rather whether the difference between np and the actual number of observations is statistically significant. Such significance tests can be found in any standard textbook on statistics in the case for which all n observations have to do with the same predicted probability p . The present paper considers the following more general setting.

Suppose we have n observations C_1, C_2, \dots, C_n of the outcomes of Bernoulli trials with corresponding predicted probabilities of success, say P_1, P_2, \dots, P_n . For instance, each P_k could be a classifier’s probabilistic score and the corresponding C_k could be the indicator of correct classification, with $C_k = 1$ when the classification is correct and $C_k = 0$ when the classification is incorrect (so C_k could also be regarded as a class label, where class 1 corresponds to “the classifier succeeded” and class 0 corresponds to “the classifier erred”). We would then want to test the hypothesis

$$C_k \sim \text{Bernoulli}(P_k) \tag{1}$$

for all $k = 1, 2, \dots, n$; the null hypothesis (1) is the same as that considered in the previous paragraph when $P_1 = P_2 = \dots = P_n = p$. Let us reorder the samples (preserving the pairing of C_k with P_k for every k) such that $P_1 \leq P_2 \leq \dots \leq P_n$, with any ties ordered randomly, perturbing so that $P_1 < P_2 < \dots < P_n$.

The canonical graphical method for assessing (1) is to bin P_1, P_2, \dots, P_n into some number — say m — of disjoint, abutting intervals indexed by I_1, I_2, \dots, I_m , and calculate both the average of P_k and the average of C_k for each bin:

$$A_j = \frac{1}{\#I_j} \sum_{k \in I_j} P_k \quad (2)$$

and

$$B_j = \frac{1}{\#I_j} \sum_{k \in I_j} C_k \quad (3)$$

for $j = 1, 2, \dots, m$, where $\#I_j$ is the number of integer indices in I_j . If the probabilistic predictions are well-calibrated, then A_j and B_j will be close for $j = 1, 2, \dots, m$. The conventional visual means of displaying whether they are close is known as a “reliability diagram” or “calibration plot,” which plot the pairs (A_j, B_j) for $j = 1, 2, \dots, m$, along with the line connecting the origin $(0,0)$ to the point $(1,1)$; a pair (A_j, B_j) falls on that line precisely when $A_j = B_j$. Copious examples of such reliability diagrams are available in the figures below, as well as in the works of [1], [2], [3], [4], [6], [7], [8], [9], [10], and many others; those works consider applications ranging from weather forecasting to medical prognosis to fairness in criminal justice to quantifying the uncertainty in predictions of artificial neural networks. An approach closely related to reliability diagrams is to smooth over the binning using kernel density estimation, as discussed by [1], [10], and others.

A common concern in diagnostics for calibration and reliability is the selection of widths for bins or for convolutional kernels in kernel density estimation: which width is best? Conveniently, this question never arises with the plots of cumulative differences suggested in the present paper, as they avoid any binning, kernel density estimation, or other procedures for smoothing or regularization. The present paper highlights the utility of cumulative plots, at least when data is reasonably scarce for the assessment of calibration.

Other works, such as Section 3.2 of [6] and Chapter 8 of [10], also point to the utility of cumulative reliability diagrams and plots somewhat similar to those in the present paper. The particular plots proposed below focus on calibration specifically, encoding miscalibration directly as the slopes of secant lines for the graphs. Such plots lucidly depict miscalibration with significant quantitative precision. Popular graphical methods for assessing calibration appear not to leverage the key to the approach advocated below, namely that slope is easy to assess visually even when the constant offset of the graph (or portion of the graph under consideration) is arbitrary and meaningless.

The following, Section 2, details the construction of the plots of cumulative differences. Then, Section 3 presents several examples of such plots alongside classical reliability diagrams. Finally, Section 4 concludes the paper with a brief discussion of the results and their consequences.

2 Methods

We adopt the notation introduced above, with n observations C_1, C_2, \dots, C_n of the outcomes of Bernoulli trials with corresponding predicted probabilities P_1, P_2, \dots, P_n ; we want to test the hypothesis (1), via a graphical display of cumulative differences. We order the samples (preserving the pairing of C_k with P_k for every k) such that $P_1 \leq P_2 \leq \dots \leq P_n$, ordering any ties at random, perturbed so that $P_1 < P_2 < \dots < P_n$.

The cumulative function is

$$F(p) = \frac{1}{n} \sum_{P_k \leq p} P_k. \quad (4)$$

An empirical estimate is

$$E(p) = \frac{1}{n} \sum_{P_k \leq p} C_k = \frac{\#\{k : P_k \leq p \text{ and } C_k = 1\}}{n}. \quad (5)$$

We will plot the difference between the following sequences:

$$F_k = F(P_k) = \frac{1}{n} \sum_{j=1}^k P_j \quad (6)$$

and

$$E_k = E(P_k) = \frac{1}{n} \sum_{j=1}^k C_j = \frac{\#\{j : 1 \leq j \leq k \text{ and } C_j = 1\}}{n} \quad (7)$$

for $k = 1, 2, \dots, n$.

Although the accumulation from lower values for p in (4) and (5) might appear to overwhelm the contributions from higher values for p , a plot of $E(p) - F(p)$ as a function of k with $p = P_k$ will reflect calibration problems for any value of p solely in slopes that deviate significantly from 0; problems accumulated from earlier, lower values of p pertain only to the constant offset from 0, not to the slope deviating from 0. Indeed, the increment in the expected difference $E_j - F_j$ from $j = k - 1$ to $j = k$ is

$$\text{Expectation}[(E_k - F_k) - (E_{k-1} - F_{k-1})] = \frac{\tilde{P}_k - P_k}{n}, \quad (8)$$

where \tilde{P}_k is the probability that the outcome is a success, that is, the probability that $C_k = 1$; thus, on a plot with the values for k spaced $1/n$ apart, the slope from $j = k - 1$ to $j = k$ is

$$\Delta_k = \tilde{P}_k - P_k. \quad (9)$$

Miscalibration for the probabilities near P_k occurs when Δ_k is significantly nonzero, that is, when the slope of the plot of $E_k - F_k$ deviates significantly from horizontal over a significantly long range.

To reiterate: *miscalibration over a contiguous range of P_k is the slope of the secant line for the plot of $E_k - F_k$ as a function of $\frac{k}{n}$ over that range, aside from the expected random fluctuations discussed next.*

The plot of $E_k - F_k$ as a function of k/n automatically includes some “error bars” courtesy of the discrepancy $E_k - F_k$ fluctuating randomly as the index k increments. Of course, the standard deviation of a Bernoulli variate whose expected value is P_k is $\sqrt{P_k(1 - P_k)}$ — smaller both for P_k near 0 and for P_k near 1. To indicate the size of the fluctuations, the plots should include a triangle centered at the origin whose height above the origin is $1/n$ times the standard deviation of the sum of independent Bernoulli variates with success probabilities P_1, P_2, \dots, P_n ; thus, the height of the triangle above the origin (where the triangle itself is centered at the origin) is $\sqrt{\sum_{k=1}^n P_k(1 - P_k)}/n$. The expected deviation from 0 of $|E_k - F_k|$ (at any specified value for k) is no greater than this height, under the assumption that the samples C_1, C_2, \dots, C_n are draws from independent Bernoulli distributions with the correct success probabilities P_1, P_2, \dots, P_n , that is, under the null hypothesis (1). The triangle is similar to the classic confidence bands around an empirical cumulative distribution function given by Kolmogorov and Smirnov, as reviewed by [5].

In addition to noting the size of the triangle at the origin, interpreting such plots of the cumulative difference $(E_k - F_k)$ between observed and expected values of ordered Bernoulli variates does require careful attention to one caveat: avoid hallucination of minor miscalibrations where in fact the calibration is good! The sample paths of random walks and Brownian motion can look surprisingly non-random (drifting?) quite often for short stints. The most trustworthy detections of miscalibration are long ranges (as a function of k/n) of steep slopes for $E(P_k) - F(P_k)$. The triangles centered at the origins of the plots give a sense of the length scale for variations that are statistically significant.

For all plots, whether cumulative or classical, bear in mind that even at 95% confidence, one in twenty detections is likely to be false. So, if there are a hundred bins, each with a 95% confidence interval, the reality is likely to violate around 5 of those confidence intervals. Beware when conducting multiple tests of significance (or be sure to adjust the confidence level accordingly)!

3 Results

Via several numerical examples, we illustrate the methods of the previous section together with the conventional diagrams discussed in the introduction. The figures display the classical calibration plots as well as both the plots of cumulative differences and the exact expectations in the absence of noise from random sampling. To generate the figures, we specify values for P_1, P_2, \dots, P_n and for $\tilde{P}_1, \tilde{P}_2, \dots, \tilde{P}_n$ differing from P_1, P_2, \dots, P_n , then independently draw C_1, C_2, \dots, C_n from the Bernoulli distributions with parameters $\tilde{P}_1, \tilde{P}_2, \dots, \tilde{P}_n$, respectively. Ideally the plots would show how and where $\tilde{P}_1, \tilde{P}_2, \dots, \tilde{P}_n$ differs from P_1, P_2, \dots, P_n . The appendix considers the case in which $\tilde{P}_k = P_k$ for all $k = 1, 2, \dots, n$.

The top rows of the figures plot $E_k - F_k$ from (6) and (7) as a function of k/n , with the rightmost plot displaying its noiseless expected value rather than using the samples C_1, C_2, \dots, C_n . In each of these plots, the upper axis specifies k/n , while the lower axis specifies P_k for the corresponding value of k . The middle two rows of the figures plot the pairs $(A_1, B_1), (A_2, B_2), \dots, (A_m, B_m)$ from (2) and (3), with the rightmost plots using an equal number of samples per bin. The left and right plots in the middle rows of Figures 1–3 are in fact identical, since P_1, P_2, \dots, P_n are equispaced for those examples (so that equally wide bins contain equal numbers of samples). The bottom rows of the figures again plot pairs $(A_1, B_1), (A_2, B_2), \dots, (A_n, B_n)$ from (2) and (3), but this time using their noiseless expected values rather than using the samples C_1, C_2, \dots, C_n .

Perhaps the simplest, most straightforward method to gauge uncertainty in the binned plots is to vary the number of bins and observe how the plotted values vary. All figures displayed employ this method, with the number of bins increased in the second rows of plots beyond the number of bins in the third rows of plots. There are many alternatives; among the most popular is to include error bars resulting from the various resampling schemes (such as the bootstrap) proposed by [2], or to display the bin frequencies as suggested, for example, by [8]. Other possibilities often involve kernel density estimation, as suggested, for example, by [1] and [10]. All such methods require selecting widths for the bins or kernel smoothing; avoiding having to make what is a necessarily somewhat arbitrary choice is possible by varying the widths, as done in the plots of the present paper. Chapter 8 of [10] comprehensively reviews the extant literature.

We may set the widths of the bins such that either (1) the average of P_k for k in each bin is approximately equidistant from the average of P_k for k in each neighboring bin or (2) the range of k for every bin has the same width. Both options are natural; the first is the canonical choice, whereas the second ensures that error bars would be roughly the same size for every bin. The figures display both possibilities, with the first on the left and the second on the right. Setting the number of bins together with either of these choices fully specifies the bins. As discussed earlier, we vary the number of bins since there is no perfect setting — using fewer bins offers estimates with higher confidence yet limits the resolution for detecting miscalibration and for assessing the dependence of calibration as a function of P_k .

Figures 1–3 all draw from the same underlying distribution that deviates linearly as a function of k from the distribution of P_k , and P_1, P_2, \dots, P_n are equispaced; Figure 1 sets $n = 10,000$, Figure 2 sets $n = 1,000$, and Figure 3 sets $n = 100$. All plots, whether cumulative or conventional, appear to work well in Figures 1 and 2. However, the conventional plots become increasingly problematic as n becomes 100 in Figure 3, whereas the cumulative plot still detects roughly the right level of miscalibration for $0 \lesssim P_k \lesssim 0.2$ and $0.8 \lesssim P_k \lesssim 1$; the cumulative plot indicates that too little data is available for $0.2 \lesssim P_k \lesssim 0.8$ to detect any statistically significant miscalibration in that range of P_k . Overall, the cumulative plots seem more informative (or at least easier to interpret) in Figures 1–3, but only mildly.

Figures 4–6 all draw from the same underlying distribution that is overconfident (lying above the perfectly calibrated ideal), with the overconfidence peaking for P_k around 0.25 (aside from a perfectly calibrated notch right around 0.25), where P_k is proportional to $(k - 0.5)^2$; Figure 4 sets $n = 10,000$, Figure 5 sets $n = 1,000$, and Figure 6 sets $n = 100$. All plots, whether cumulative or conventional, work well enough in Figures 4 and 5, though the reliability diagrams might be mistakingly misleading relative to the exact expectations, at least without diligent attention to the significant variation with the number of bins. The plots, whether cumulative or conventional, reveal similar information in Figure 6, too, though the reliability diagram with an equal number of samples per bin provides more reliable estimates than the other reliability diagram. The cumulative plot is perhaps the easiest to interpret: the miscalibration is significant for $0.1 \lesssim P_k \lesssim 0.23$ and $0.27 \lesssim P_k \lesssim 0.6$, with about the correct amount of miscalibration (the amount is correct since the secant lines have the expected slopes).

Figures 7–9 all draw from the same, relatively complicated underlying distribution, with P_k being proportional to $\sqrt{k - 0.5}$; Figure 7 sets $n = 10,000$, Figure 8 sets $n = 1,000$, and Figure 9 sets $n = 100$. The cumulative plots capture more of the oscillations in the miscalibration, as do to some extent the reliability diagrams with an equal number of samples per bin; however, the variations in the reliability diagrams could be difficult to interpret without access to the ground-truth exact expectations.

The following section concludes the discussion of these results and their implications. The appendix provides further illustrative examples.

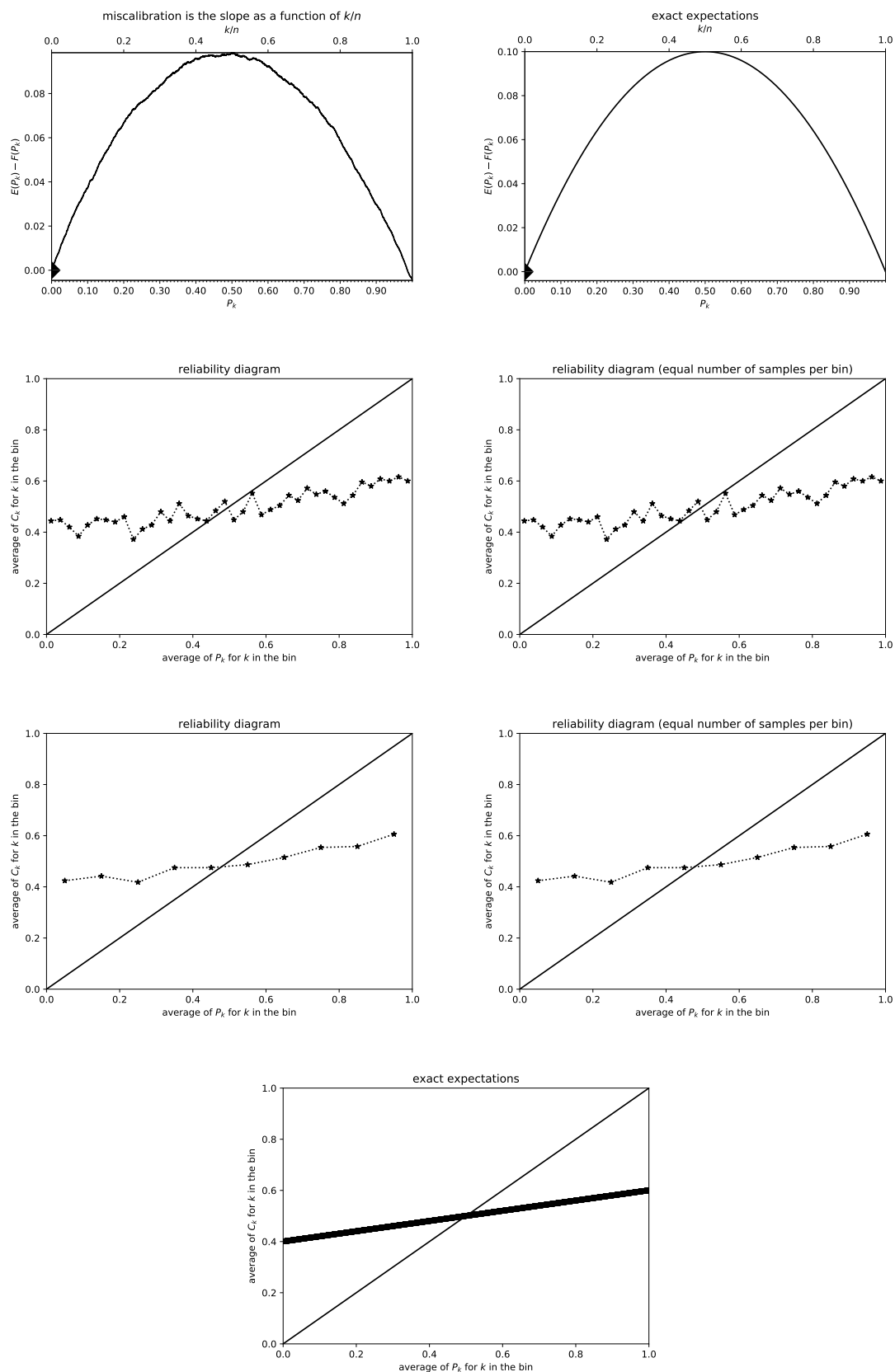


Figure 1: $n = 10,000$; P_1, P_2, \dots, P_n are equispaced

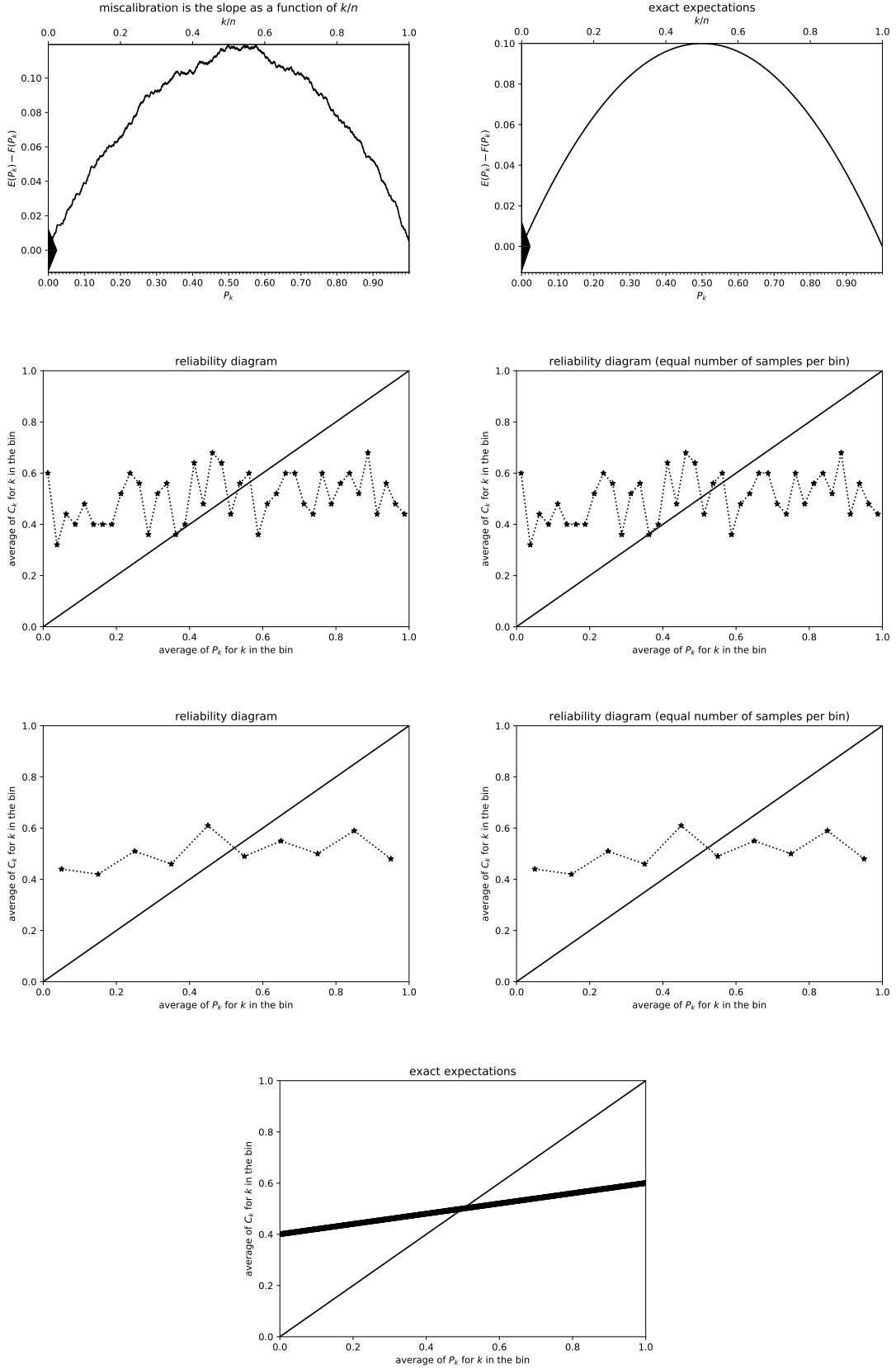


Figure 2: $n = 1,000$; P_1, P_2, \dots, P_n are equispaced

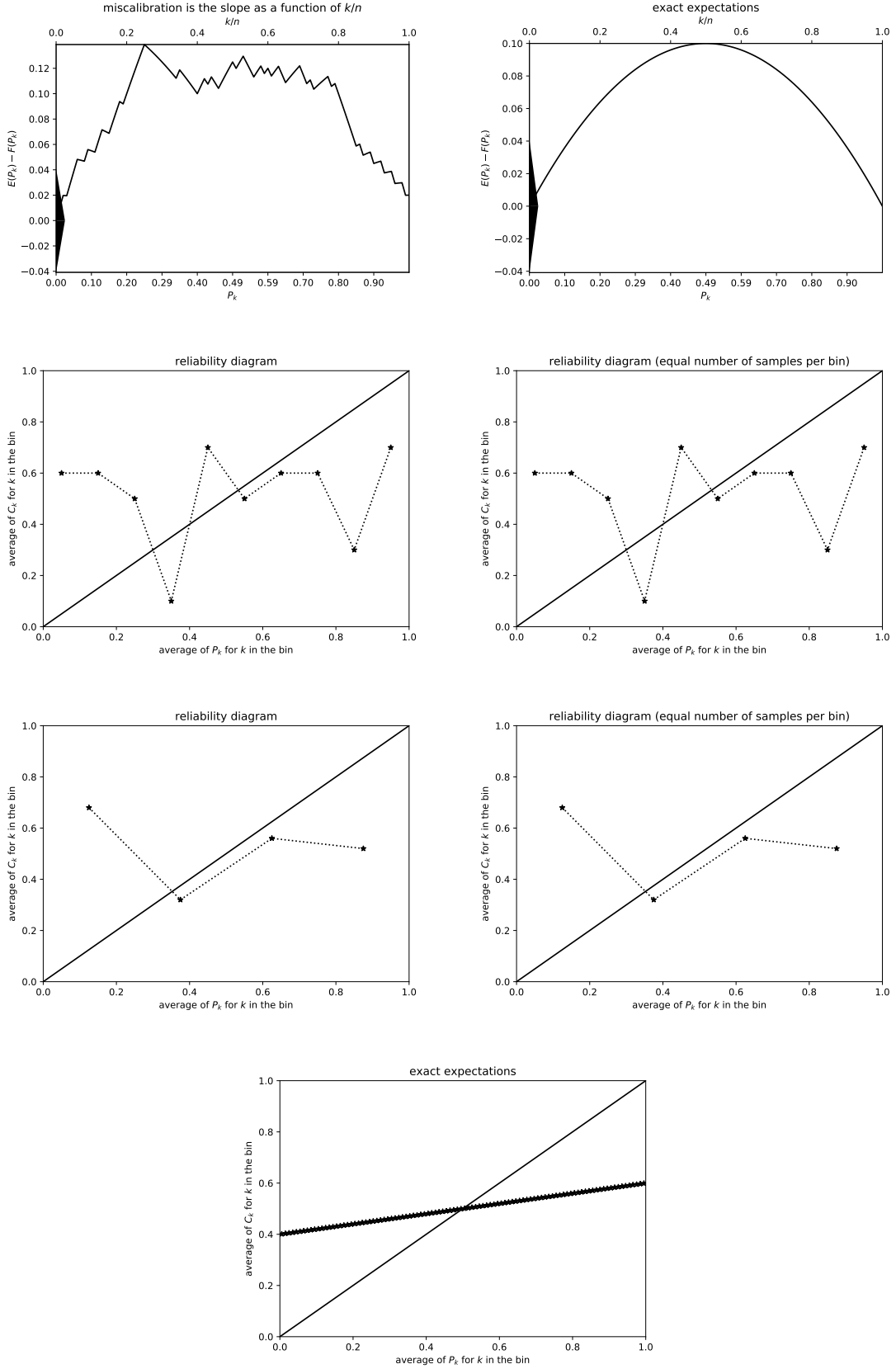


Figure 3: $n = 100$; P_1, P_2, \dots, P_n are equispaced

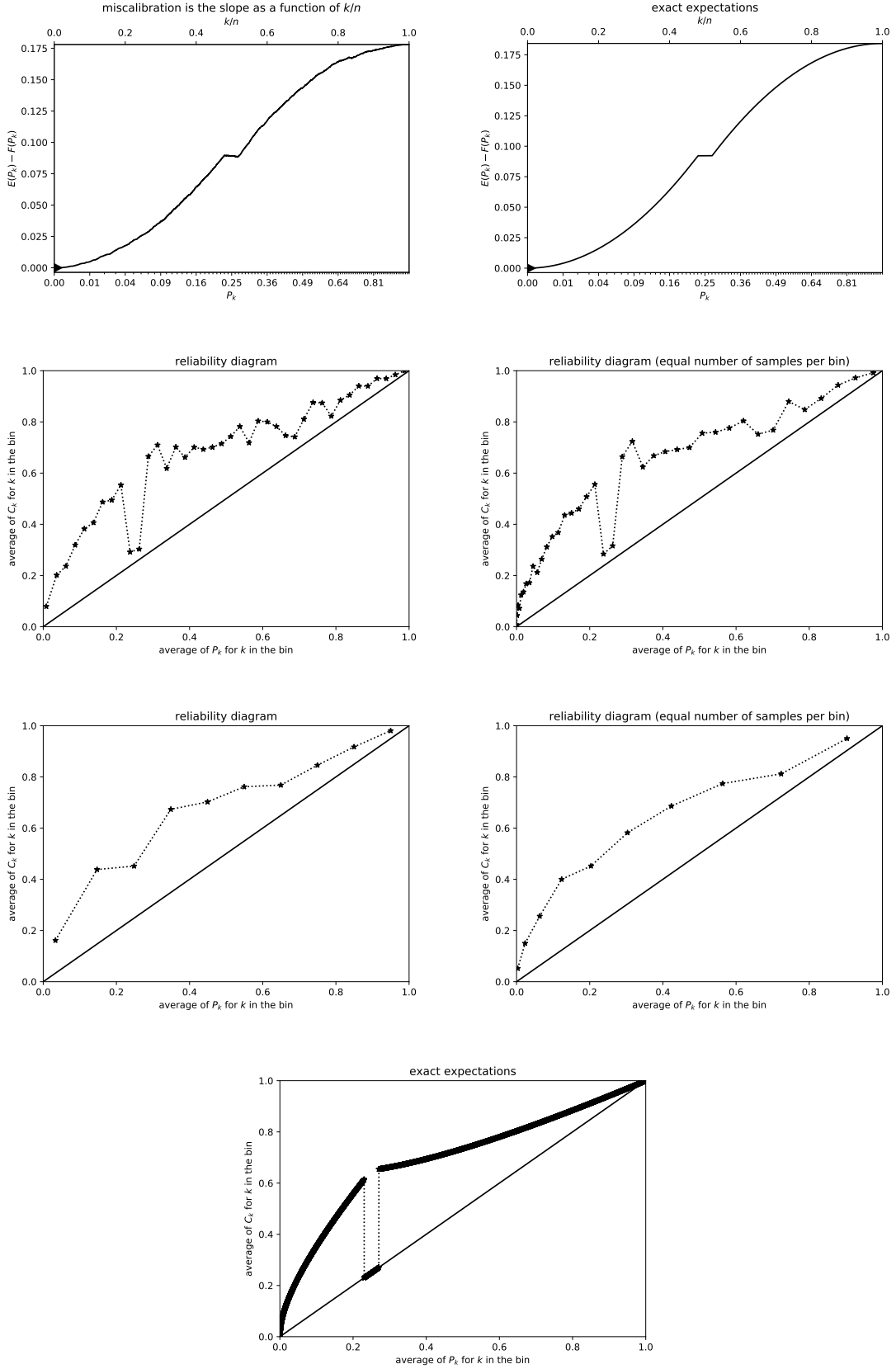


Figure 4: $n = 10,000$; P_1, P_2, \dots, P_n are denser near 0

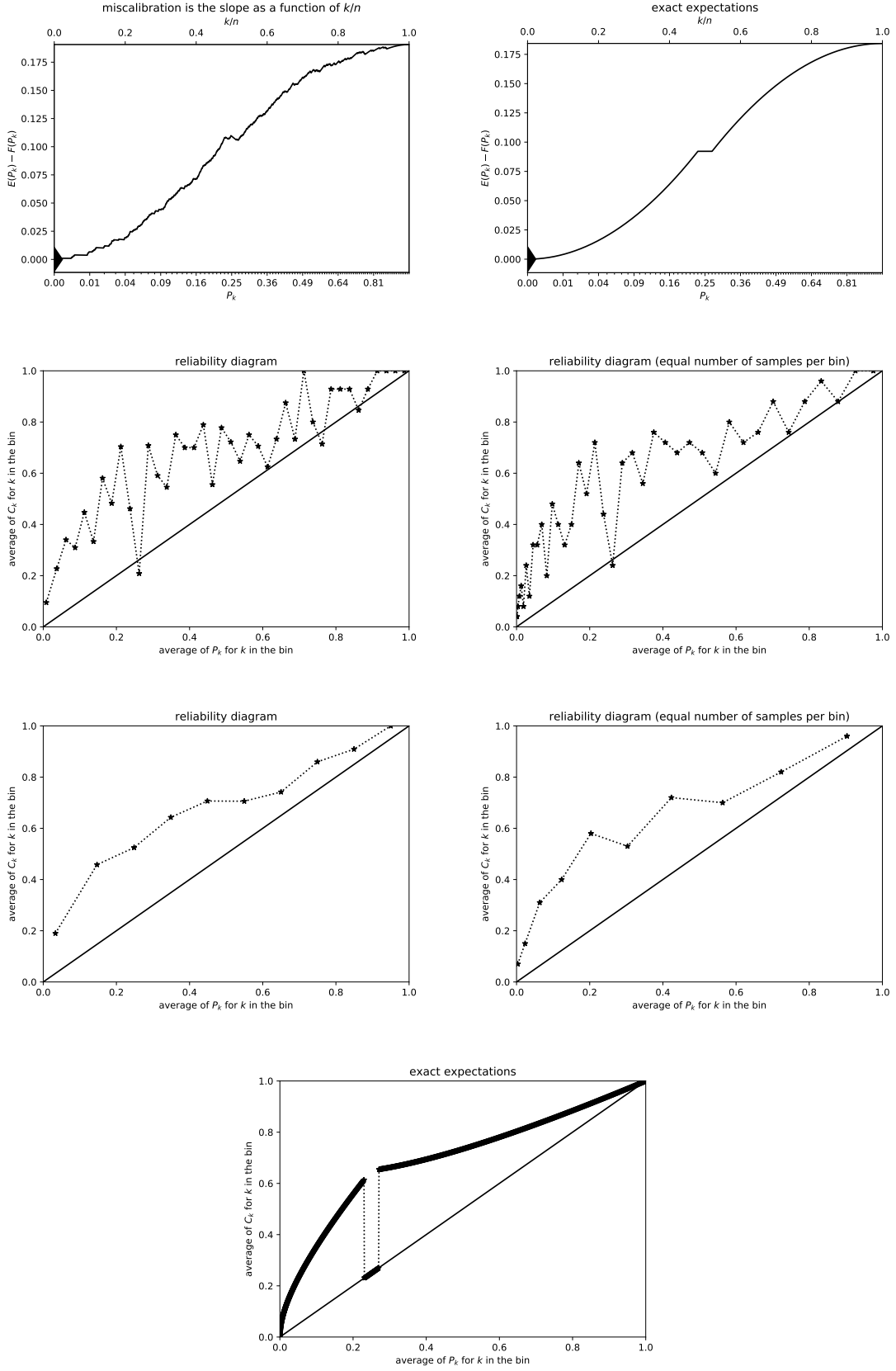


Figure 5: $n = 1,000$; P_1, P_2, \dots, P_n are denser near 0

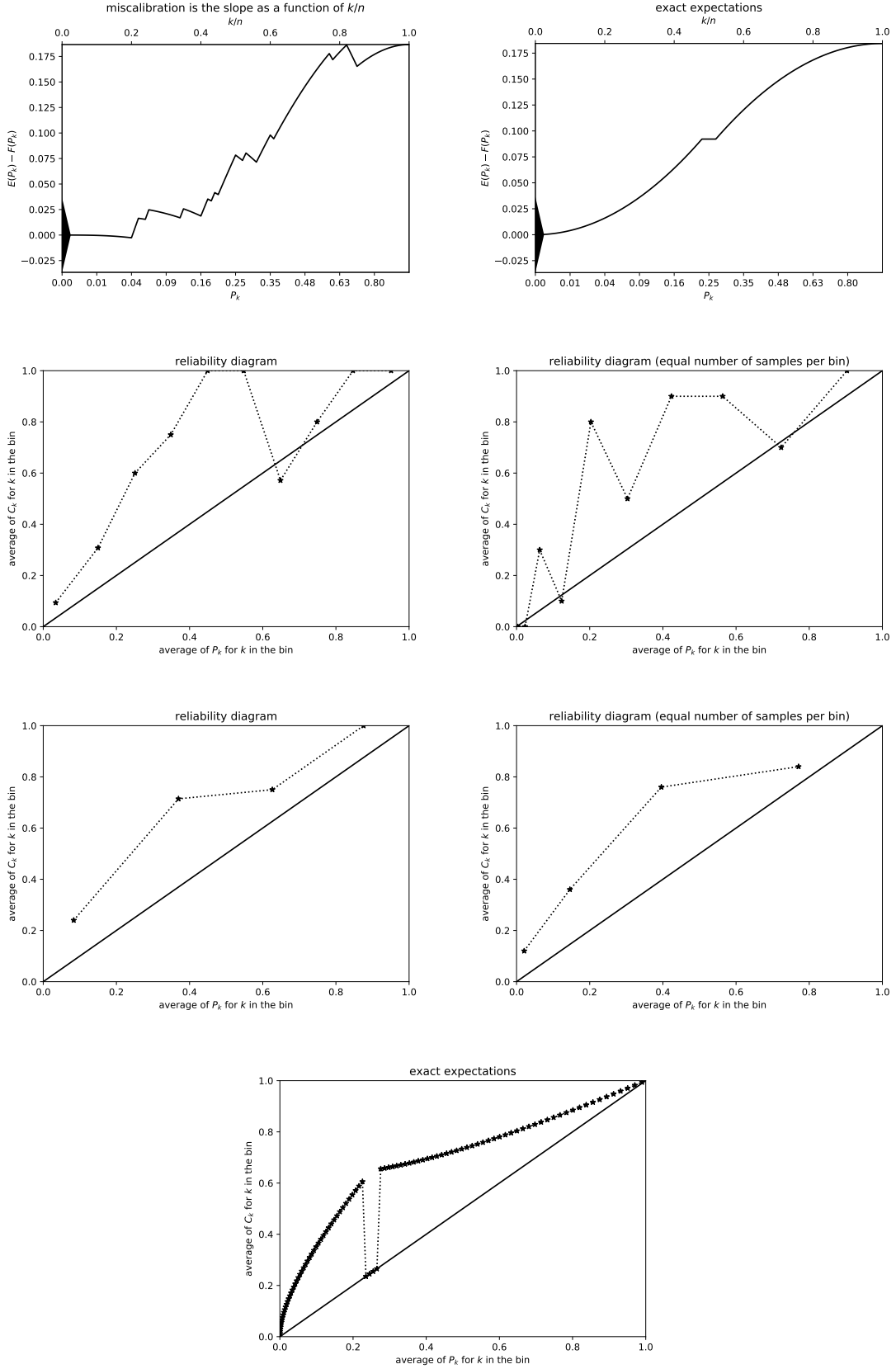


Figure 6: $n = 100$; P_1, P_2, \dots, P_n are denser near 0

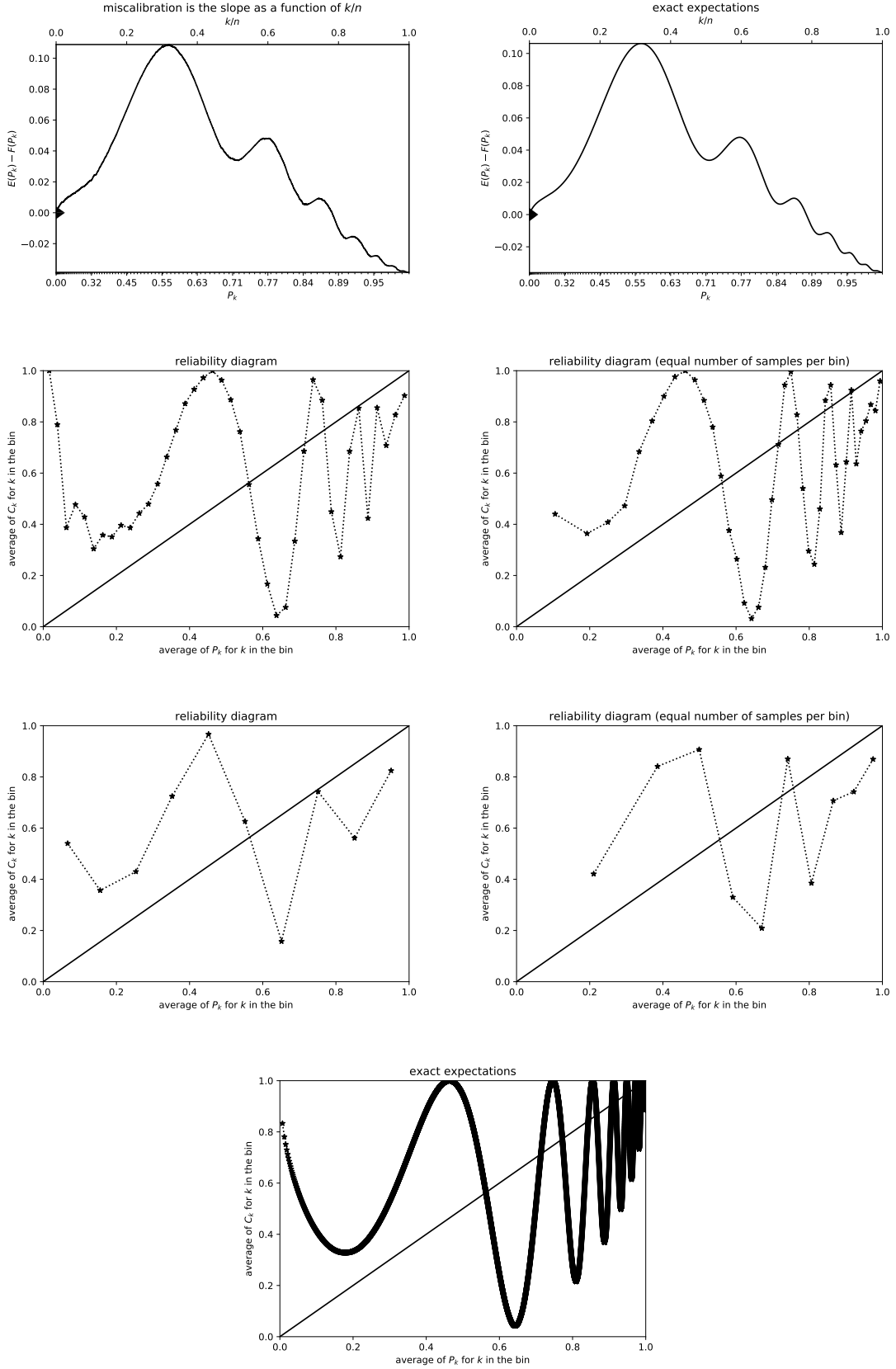


Figure 7: $n = 10,000$; P_1, P_2, \dots, P_n are denser near 1

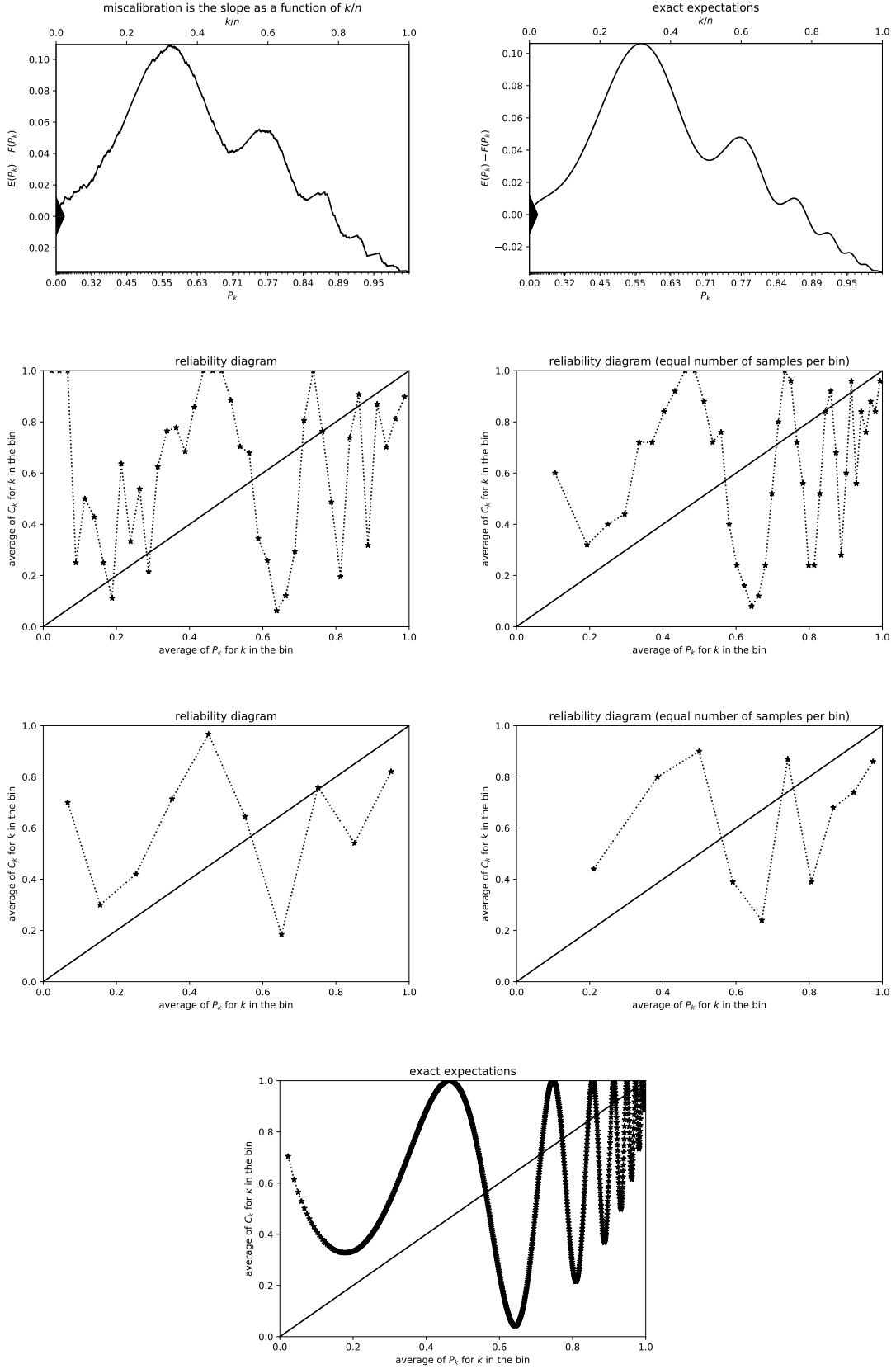


Figure 8: $n = 1,000$; P_1, P_2, \dots, P_n are denser near 1

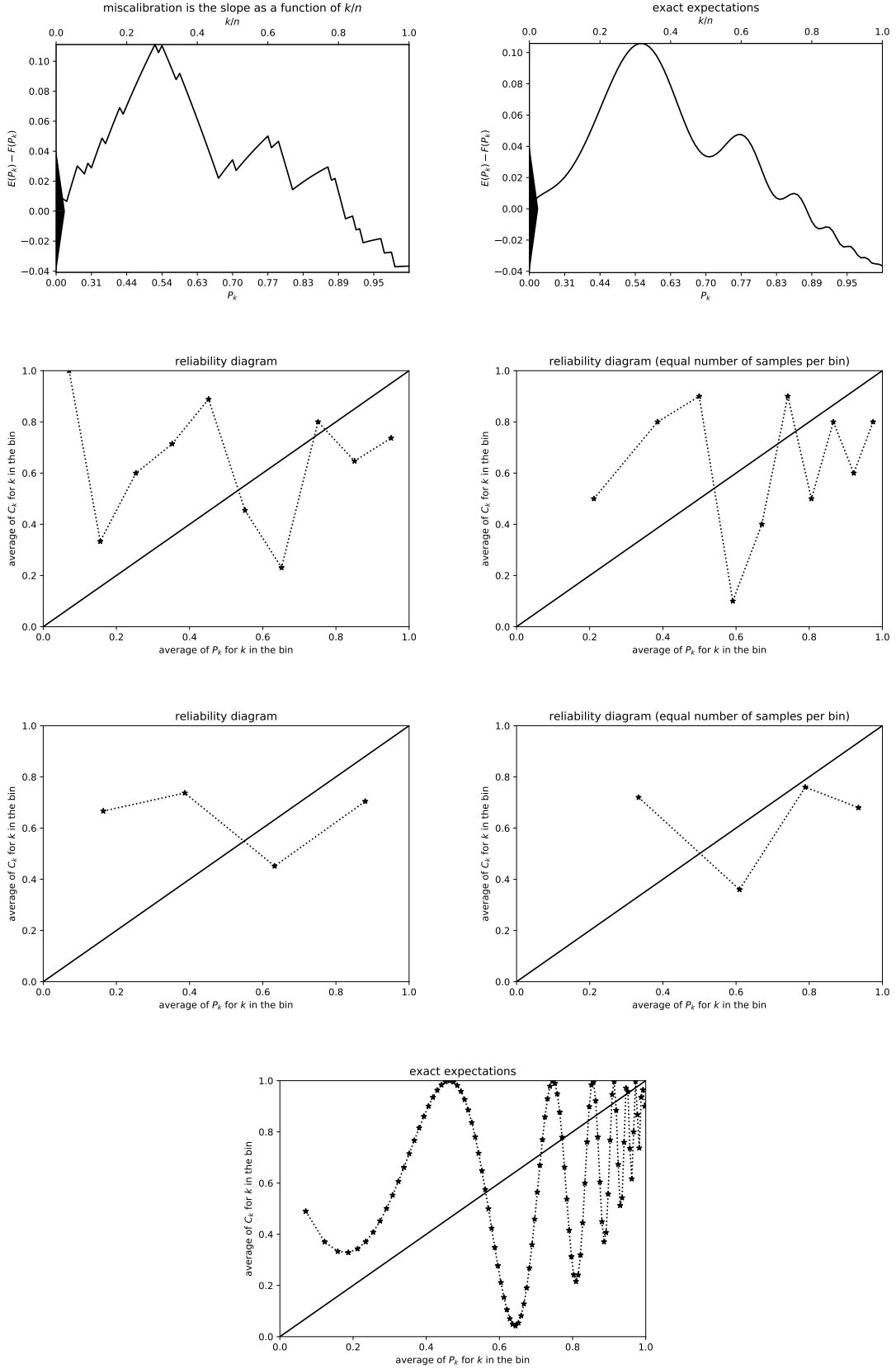


Figure 9: $n = 100$; P_1, P_2, \dots, P_n are denser near 1

4 Discussion and conclusion

Graphing the cumulative differences between observed and expected values of the sorted predictions sidesteps having to make an arbitrary choice of widths for bins or convolutional kernels — a choice which is necessary in the canonical reliability diagrams and their variants. As reviewed above, the selection can also be made somewhat less arbitrary by constructing multiple plots with varying numbers of bins or by adding estimates of errors with resampling schemes such as the bootstrap. Choosing between the cumulative plot and the more complicated conventional reliability diagrams may be merely a matter of convenience and personal preference. The plot of cumulative differences encodes miscalibration directly as the slope of secant lines for the graph, and such slope is easy to perceive independent of any irrelevant constant offset of a secant line; the graph of cumulative differences very directly enables detection and quantification of miscalibration, along with identification of the ranges of miscalibrated probabilities. The cumulative differences estimate the distribution of miscalibration fully nonparametrically, letting the data samples speak for themselves (or nearly for themselves — the triangle at the origin helps convey the scale of a driftless random walk’s expected random fluctuations). As seen in the figures, the graph of cumulative differences automatically adapts its resolving power to the distribution of miscalibration and sampling, not imposing any artificial grid of bins or set-width smoothing kernel, unlike the conventional reliability diagrams and calibration plots.

Acknowledgements

We would like to thank Tiffany Cai, Joaquin Candela, Kenneth Hung, Mike Rabbat, and Adina Williams.

A Appendix: Random walks

This appendix provides figures — Figures 10–12 — analogous to those presented in Section 3, but with the observations drawn from the same predicted probabilities used to generate the graphs, so that the discrepancy from perfect calibration should be statistically insignificant. More precisely, Figures 10–12 all set P_k to be proportional to $(k - 0.5)^2$ and draw C_1, C_2, \dots, C_n from independent Bernoulli distributions with expected success probabilities P_1, P_2, \dots, P_n , respectively; this corresponds to setting $\tilde{P}_k = P_k$ for all $k = 1, 2, \dots, n$, in the numerical experiments of Section 3. Figures 10, 11, and 12 consider $n = 10,000$, $n = 1,000$, and $n = 100$, respectively. Please note that the ranges of the vertical axes for the top rows of plots are drastically smaller in Figures 10–12 than in Figures 1–9. The leftmost topmost plots in Figures 10–12 look like driftless random walks; in fact, they really are driftless random walks. The variations of the graphs are comparable to the heights of the triangles centered at the origins. Comparing the second rows with the third rows shows that the deviations from perfect calibration are consistent with expected random fluctuations. Indeed, all plots in this appendix depict only small deviations from perfect calibration, as expected (and as desired).

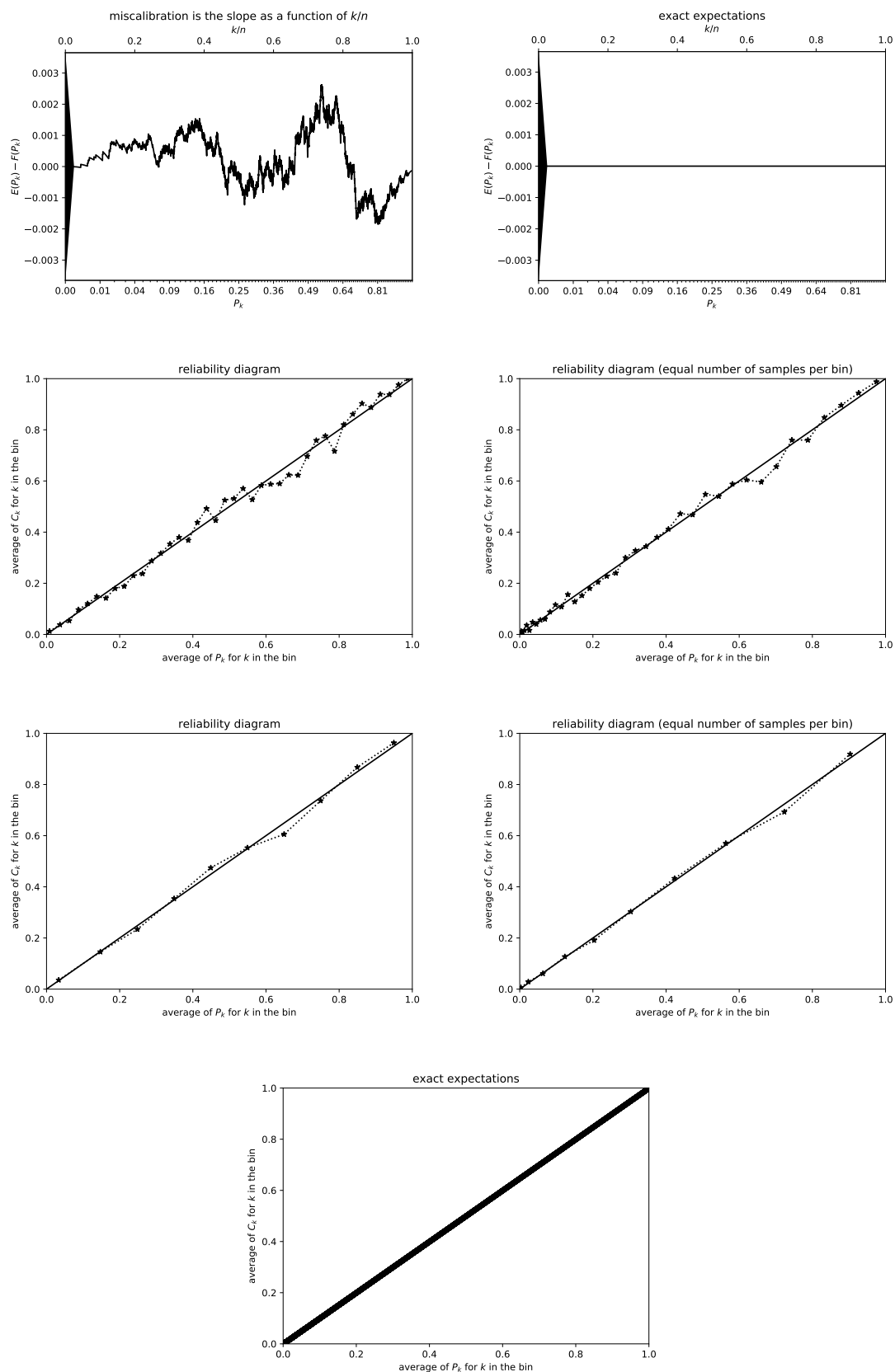


Figure 10: $n = 10,000$; P_1, P_2, \dots, P_n are denser near 0

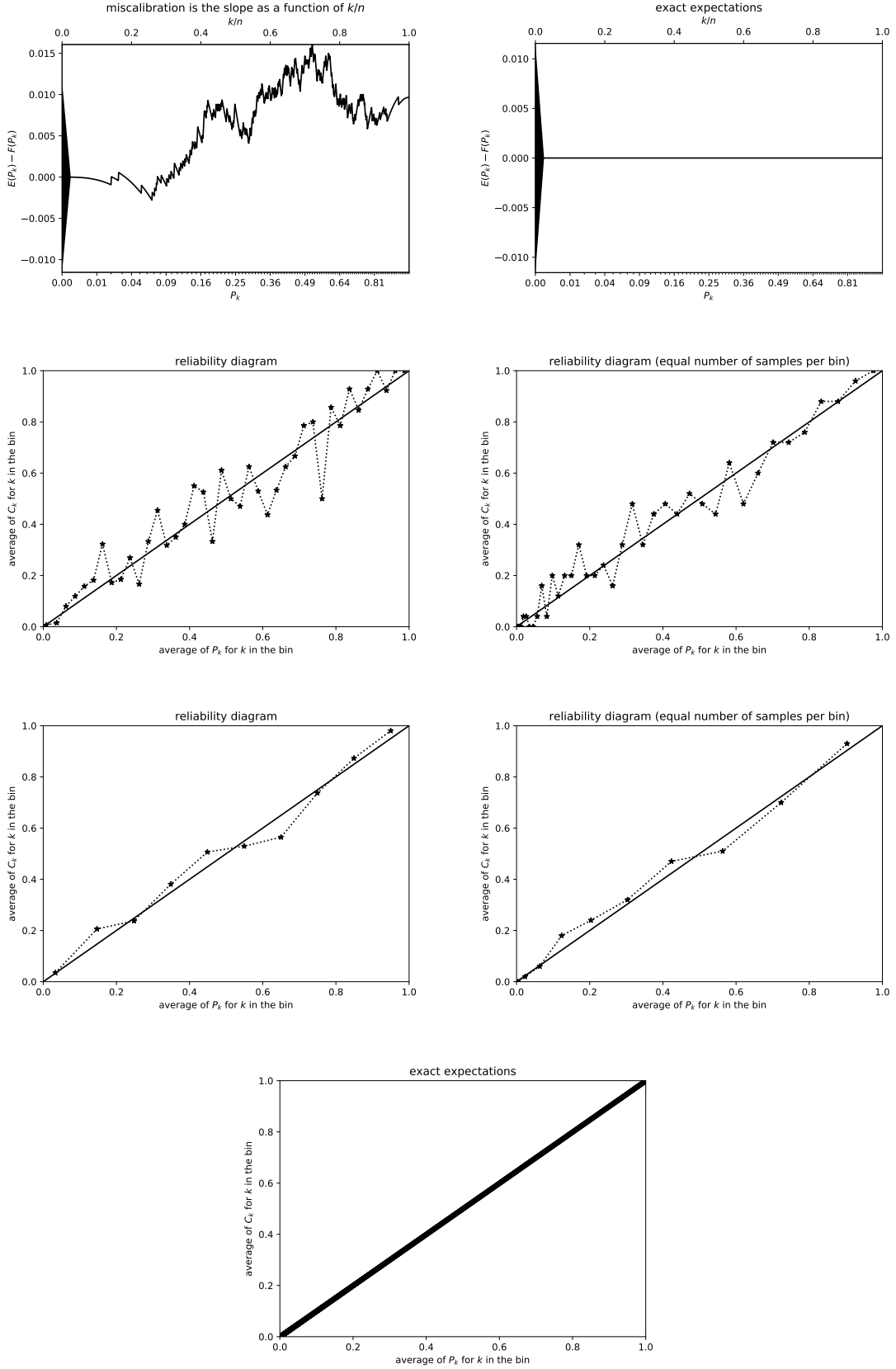


Figure 11: $n = 1,000$; P_1, P_2, \dots, P_n are denser near 0

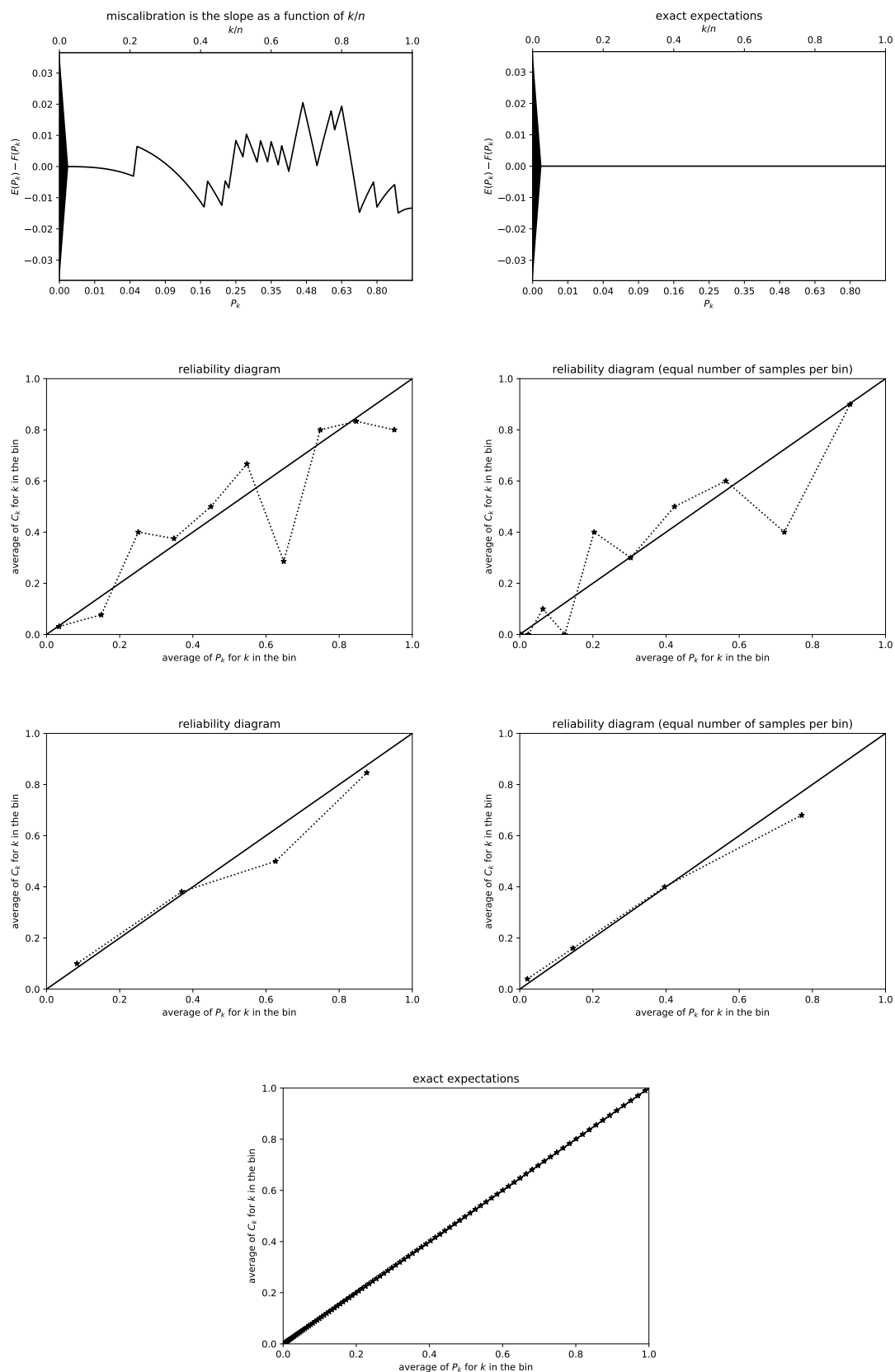


Figure 12: $n = 100$; P_1, P_2, \dots, P_n are denser near 0

References

- [1] J. BRÖCKER, *Some remarks on the reliability of categorical probability forecasts*, Mon. Weather Rev., 136 (2008), pp. 4488–4502.
- [2] J. BRÖCKER AND L. A. SMITH, *Increasing the reliability of reliability diagrams*, Weather Forecast., 22 (2007), pp. 651–661.
- [3] S. CORBETT-DAVIES, E. PIERSON, A. FELLER, S. GOEL, AND A. HUQ, *Algorithmic decision making and the cost of fairness*, in Proc. 23rd ACM SIGKDD Int. Conf. Knowl. Disc. Data Min., Assoc. Comput. Mach., 2017, pp. 797–806.
- [4] C. S. CROWSON, E. J. ATKINSON, AND T. M. THERNEAU, *Assessing calibration of prognostic risk scores*, Stat. Methods Med. Res., 25 (2016), pp. 1692–1706.
- [5] K. A. DOKSUM, *Some graphical methods in statistics: a review and some extensions*, Statist. Neerl., 31 (1977), pp. 53–68.
- [6] T. GNEITING, F. BALABDAOUI, AND A. E. RAFTERY, *Probabilistic forecasts, calibration, and sharpness*, J. Royal Stat. Soc. B, 69 (2007), pp. 243–268.
- [7] C. GUO, G. PLEISS, Y. SUN, AND K. Q. WEINBERGER, *On calibration of modern neural networks*, Proc. Mach. Learn. Res., 70 (2017), pp. 1321–1330. Proc. 34th Int. Conf. Mach. Learn.
- [8] A. H. MURPHY AND R. L. WINKLER, *Diagnostic verification of probability forecasts*, Int. J. Forecast., 7 (1992), pp. 435–455.
- [9] J. VAICENAVICIUS, D. WIDMANN, C. ANDERSSON, F. LINDSTEN, J. ROLL, AND T. B. SCHÖN, *Evaluating model calibration in classification*, Proc. Mach. Learn. Res., 89 (2019), pp. 3459–3467. Proc. 22nd Int. Conf. Artif. Intell. Stat.
- [10] D. S. WILKS, *Statistical Methods in the Atmospheric Sciences*, vol. 100 of International Geophysics, Academic Press, 3rd ed., 2011.